Journal of Quantitative Spectroscopy & Radiative Transfer 220 (2018) 84–96

Contents lists available at ScienceDirect

Journal of Quantitative Spectroscopy & Radiative Transfer

journal homepage: www.elsevier.com/locate/jqsrt

Cloud information content in EPIC/DSCOVR's oxygen A- and B-band channels: A physics-based approach

Anthony B. Davis[a,*], Nicolas Ferlay[b], Quentin Libois[c], Alexander Marshak[d], Yuekui Yang[d], Qilong Min[e]

[a] Jet Propulsion Laboratory, California Institute of Technology, Pasadena, CA, USA
[b] Laboratoire d'Optique Atmosphérique CNRS, Université Lille-1, Villeneuve d'Ascq, France
[c] CNRM, Université de Toulouse, Météo-France, CNRS, 42, Avenue Gaspard Coriolis, Toulouse, 31100, France
[d] NASA Goddard Space Flight Center Climate and Radiation Laboratory, Greenbelt, MD, USA
[e] Atmospheric Sciences Research Center, State University of New York at Albany, Albany, NY, USA

ARTICLE INFO

Article history:
Received 8 May 2018
Revised 7 September 2018
Accepted 7 September 2018
Available online 8 September 2018

Keywords:
Multiple scattering
Oxygen A-band
Oxygen B-band
Radiative transfer
Remote sensing
Cloud top height
Geometrical cloud thickness
DSCOVR
EPIC
Retrieval uncertainty quantification

ABSTRACT

In a companion paper [Davis et al., *JQSRT* 216, 6–16 (2018)], we used a *numerical* 1D radiative transfer (RT) model and the *statistical* formalism of optimal estimation to quantify cloud information content in the O_2 A- and B-band channels of the Earth Polychromatic Imaging Camera (EPIC) on the Deep Space Climate ObserVatoRy (DSCOVR) platform that images the Earth's sunlit hemisphere from the vantage of the Lagrange-1 point. These two pairs of "in-band" and nearby "reference" radiances are combined into differential optical absorption spectroscopic (DOAS) ratios for both A- and B-bands, from which one can derive, in principle, both cloud top height (CTH) and cloud geometric thickness (CGT). However, Davis et al. show that under most circumstances, there is much redundancy between the two DOAS ratios and, in practice, only CTH can be reliably and accurately retrieved. Here, we derive a simplified *analytical* 1D RT model for the DOAS ratios to gain *physical* insights as well as quantify both the CTH retrieval bias from neglecting in-cloud absorption and the impact of measurement error on CTH and CGT retrievals. Using this alternative approach, we again show that only CTH can be inferred reliably when unavoidable measurement error is factored in. Finally, our new theoretical developments are related to a recently uncovered invariance property of the mean path cumulated by light in arbitrarily-shaped optical media of arbitrary opacity with arbitrary scattering properties, as long as it is conservative.

1. Introduction & overview

Clouds are still a poorly understood element of the Earth's climate system and, consequently, they are poorly parameterized in global climate models (GCMs)—so much so that a large part of the uncertainty about predicting future climate can be traced to this gap [1]. This fact, as troublesome as well-documented, has motivated the National Academies to list clouds as top-priority for continued and enhanced observation from space in the recently released 2017 Decadal Survey [2].

The Deep Space Climate ObserVatoRy (DSCOVR) mission [3,4] has pushed Earth observation from space literally to new heights by locating the platform near the Sun–Earth "Lagrange-1" (L_1) point, at c. 1,500,000 km from our planet in direction of the Sun—figuratively, as well. Indeed, the Earth Polychromatic Imaging Camera (EPIC) [5] is one of the two Earth-oboserving sensors on DSCOVR. EPIC images the Earth every 60 to 100 min [6] with a 2048 × 2048 pixel camera (≈8 km pixels at the center of the disc) boosting 10 narrow spectral channels sampling the UV–VIS range. Among these, the four of interest here are at the longest wavelengths: 680, 688, 764, and 780 nm. They are dedicated in particular to forming two in-band/out-of-band radiance ratios for di-oxygen's A- and B-bands. This is primarily for the purpose of determining the altitude at which the highest cloud layer occurs in every cloudy pixel.

The present investigation, described both here and in a companion paper [7], builds on a preliminary study by Yang et al. [8] who proposed an elegant method for deriving *both* cloud top height (CTHs) and cloud geometrical thickness (CGT). For single-layer cloud cover, this is a rudimentary way of profiling the cloudy atmosphere. Such information would be very helpful to cloud scientists working on GCM cloud schemes. Following Yang et al.'s the-

* Corresponding author.
E-mail address: Anthony.B.Davis@jpl.nasa.gov (A.B. Davis).

https://doi.org/10.1016/j.jqsrt.2018.09.006
0022-4073/

oretical study, we start with the assumption that EPIC has access to both pieces of cloud profile information.

In the companion paper [7], Davis et al. used a more realistic representation of the EPIC sensor. In particular, they included measurement noise, which was neglected in [8], and applied the formal information content analysis methodology of Merlin et al. [9], itself inspired by Rodgers [10] theory of optimal estimation (OE). In spite of good signal-to-noise ratios (SNRs) in the four channels, and of the reduced noise level achieved by forming the in-band/continuum radiance ratios, Davis et al. conclude that there is too much alignment of the A- and B-band responses to both cloud properties to separate them in presence of the anticipated noise. Consequently, only the dominant property (CTH) can be derived with good precision. In the jargon of OE, CGT has to be moved from an unknown element of the atmospheric "state vector" argument of the forward model to the set of atmospheric properties whose values need to be determined otherwise, within known uncertainty.

In the present study, we use a closed-form analytical model for the in-band/continuum radiance ratios instead of the computational 1D radiative transfer (RT) model used in the companion paper as a proverbial "black box." Here, we derive the simpler but analytically tractable model from the first principles of 1D RT theory, gaining insights about A- and B-band cloud observations along the way. Coming from this *physics*-based approach, we arrive at the same conclusions as in [7] about the retrievability of CTH, and not CGT, where a *statistics*-based approach was adopted in the sense of OE formalism. Moreover, the analytical model is used to quantify the bias in retrieved CTH if the impact of CGT on the signal is neglected, hence the need to make some plausible assumption about GCT to ensure not only precise but accurate retrievals of CTH.

In the next Section, we describe the 1D RT modeling framework used in this investigation, leading to our analytical approximation and shedding new light on the uncertainty budget for cloud property retrievals, with the more technical aspects described in Appendix A. The systematic (forward modeling) error incurred when neglecting in-cloud O_2 absorption is quantified in Section 3. In Section 4, we turn to the impact of random (measurement) error on retrievals, leading to a physics-based cloud information content analysis for EPIC's O_2 A- and B-band channels with CTH and CGT as remote sensing targets. We summarize our findings in §5 and discuss potentially far-reaching connections with laboratory studies of mean pathlengths that are elucidated in Appendix B.

2. Radiative transfer framework

2.1. Atmospheric optical properties

As in the companion paper, we represent the atmosphere a priori with three layers (above, inside, and below the cloud layer); see Fig. 1 in [7]. We denote the O_2 absorption coefficient, dependent on the ambient temperature T_z and pressure P_z, as $k_{O_2}(\lambda; P_z, T_z)$ at altitude z. The optical depth for absorption by di-oxygen between altitude z and the top-of-atmosphere (TOA, symbolically, $z = \infty$) along the vertical is

$$\tau_{O_2}(\lambda; z) = \int_z^\infty k_{O_2}(\lambda; P_z, T_z)\mathrm{d}z. \tag{1}$$

Following [7], we make these assumptions:

- In the O_2 lines, above- and below-cloud layers are considered purely absorbing ($\sigma_c \equiv 0$) with transmission factors dependent only on solar/viewing geometry and the amount of oxygen above cloud top and between cloud base and surface, respectively: $\tau_{O_2}(\lambda; z_{top})$, where z_{top} is CTH, and $\left[\tau_{O_2}(\lambda; z)\right]_{z_{top}-H}^{0} = \tau_{O_2}(\lambda; 0) - \tau_{O_2}(\lambda; z_{top} - H)$ with H denoting CGT.
- In the A- and B-bands as well as in the continuum, the cloud layer is therefore the only region with a non-vanishing scattering coefficient, hence single-scattering albedo (SSA).
  - Rayleigh scattering optical depths of the atmosphere, roughly 0.03 and 0.04, respectively for A- and B-band regions (reference and in-band channels), are negligible compared to all other optical depths, that is, for scattering by cloud droplets, and all the more so in the presence of absorption by O_2. Following [8], we neglect Rayleigh scattering.
  - Aerosols will generally have optical depths that are larger than for Rayleigh scattering in these spectral regions, but still nowhere near the COT values considered here. We neglect them too in order to keep our atmospheric model as close as possible to the one used by Yang et al. [8], as we will be comparing results quantitatively further on.

  SSA in the cloud layer is therefore determined only by the value of the cloud droplet scattering coefficient σ_c that, again following [8], is assumed constant, and the gaseous absorption coefficient introduced in (1). It can therefore be estimated as needed from COT τ_c, H and the values of $k_{O_2}(\lambda; P_z, T_z)$ for $z_{top} - H < z < z_{top}$. Internal variations of the SSA matter only when H becomes commensurate with the pressure scale-height (≈ 8 km).
- Finally, the surface is assumed here to be black, meaning that we limit this study to clouds above water. Yang et al. [8] assigned to the surface albedo a small but finite value for water of 0.05. In the companion paper [7], both black and highly reflective lower boundaries were examined.

In the absence of molecular and aerosol scattering distributed across the whole atmosphere, the last simplification reduces to just two the number of atmospheric layers to consider: transparent or absorbing above-cloud layer; scattering cloud layer, with or without absorption.

2.2. Spectral considerations

Fig. 1 shows the EPIC in-band filter functions $f_{in}(\lambda)$ for A- and B-bands in arbitrary units along with $\tau_{O_2}(\lambda; 0)$ from (1) on a log-scale, with more spectral detail than in Fig. 2 of [7] and more focus on the EPIC in-band channels.

Now let $f^\star_{in}(\lambda)$ denote the *normalized* filter function, i.e., $f_{in}(\lambda)/\int_{\Delta\lambda} f_{in}(\lambda)\mathrm{d}\lambda$ in nm^{-1}. In the companion paper, we used a standard correlated-k technique [11–15] to account for the spectral variability, as modulated by $f^\star_{in}(\lambda)$. Here, we switch to a simpler band-average approach [e.g., 13,16]. A- and B-band average quantities of interest are:

- the *mean* absorption optical thicknesses, $\int_{\Delta\lambda} \tau_{O_2}(\lambda; 0) f^\star_{in}(\lambda)\mathrm{d}\lambda$, yielding 1.08 for B-band and 9.56 for A-band, which seems like a good contrast in absorption strength, hence a potential for differentiating shorter and longer paths, which is precisely what is needed to sense both cloud top (with shortest paths) and cloud base (with longest paths);
- an airmass-dependent *effective* absorption optical thicknesses defined as

$$\tau^{(\Delta\lambda)}_{O_2}(M) = -\frac{1}{M}\log\left(\int_{\Delta\lambda} \exp[-M\tau_{O_2}(\lambda; 0)] f^\star_{in}(\lambda)\mathrm{d}\lambda\right), \tag{2}$$

where the so-called "airmass" factor

$$M = \frac{1}{\cos\theta_0} + \frac{1}{\cos\theta} = \frac{1}{\mu_0} + \frac{1}{\mu}, \tag{3}$$

with θ_0 and θ denoting solar (SZA) and viewing (VZA) zenith angles, respectively. For EPIC, we have $\theta \approx \theta_0$, and a typical value of M is 3, which would result from $\theta_0 \approx \cos^{-1}(\frac{2}{3}) = 48.2^\circ$.

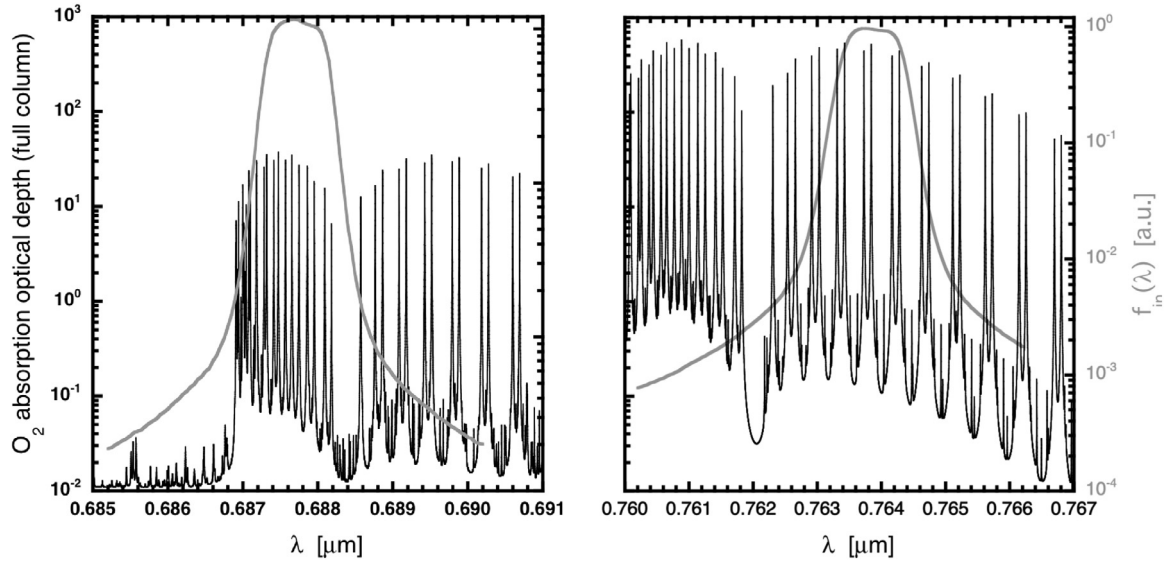

Fig. 1. In-band EPIC filter functions (in arbitrary units), with full-column O_2 absorption optical depth for the standard mid-latitude summer atmosphere in the "line-by-line" limit (wavenumber increment $\delta\nu = 0.01$ cm^{-1}): *Left:* B-band ($\delta\lambda \approx$ 0.5 pm). *Right:* A-band ($\delta\lambda \approx$ 0.6 pm).

The nonlinear average in (2) then yields effective absorption optical thickness of $\tau_{O_2}^{(B)}(3) = 0.17$ for the B-band and $\tau_{O_2}^{(A)}(3) = 0.41$ for the A-band. Fig. 2 shows the relatively weak dependence of these effective O_2 absorption optical depths on M (when $\theta = \theta_0$, over a range where sphericity effects can be safely neglected).

The latter nonlinear averaging over the orders of magnitude in spectral variability of $\tau_{O_2}(\lambda; 0)$ inside the EPIC A- and B-band filters is recommended when seeking a single absorption optical depth in the simple monochromatic representations of the EPIC signals used, as needed, further on. However, the contrast between the A- and B-bands has gone from a factor of $\approx$10 to a factor of $\approx$2, which is moreover between two relatively small optical depths characteristic of the wings of the otherwise very deep lines.

Band-average transmission models have been developed over the last decades, most famously by Elsasser, Goody, and Malkmus; see, e.g., survey by Modest [17, Ch. 10], and references therein. Indeed this continues to be an area of active research [e.g., 18–20]. The simple scheme that uses $\exp(-\tau_{O_2}^{(\Delta\lambda)}(M))$ from (2) may not be the best, even for our present purposes. Nonetheless, the band-average representation of O_2 absorption in (2) and Fig. 2 will be used, for simplicity, for numerical estimations in Fig. 3 and in §4; until then, much of the reasoning remains monochromatic. The impact of this choice will be discussed where appropriate, and we differ to a future publication the quantitative comparison of (2) with more sophisticated statistical transmission models. We only need to bear in mind here that most of the radiation that matters for the sensor response is transmitted through the optically thin parts of the filter's band-pass, i.e., the wings of the spectral lines.

We now have all the required information to compute radiances observed by EPIC at all the wavelengths of interest in A- and B-band studies. However, to understand these observations, it is important to bear in mind that it is fundamentally all about the amount of absorption by O_2 cumulated along all possible paths that sunlight can follow between injection and escape at TOA. This approach will lead us to approximate-but-analytical expressions for the EPIC signals of interest that are good enough for the present uncertainty quantification exercise, but far from satisfactory in a full physics-based retrieval algorithm.

2.3. Monochromatic formulation

Let $I_{TOA}(\lambda, \mathbf{\Omega})$ be radiance at wavelength λ leaving the TOA in direction $\mathbf{\Omega}$, in this study, toward EPIC/DSCOVR at L_1. We will use it non-dimensional "BRF" form $R_{TOA}(\lambda, \mathbf{\Omega}) = \pi I_{TOA}(\lambda, \mathbf{\Omega})/\mu_0 F_0(\lambda)$, which is the bi-directional reflection factor (BRF) of the surface-atmosphere system. The BRF is defined as the effective planar albedo were the system Lambertian, i.e., independent of $\mathbf{\Omega}_0$ ($\Omega_{0z} = \mu_0$), $\mathbf{\Omega}$ ($|\Omega_z| = \mu$), for the incoming (solar) and outgoing (view) directions, respectively, and of the relative azimuth.

In the upper (above-cloud) non-scattering region, all we need to know is solar and observational geometry. Therefore, neglecting surface reflection of light transmitted through the cloud in both directions, radiance observed from space BRF form is

$$R_{TOA}(\lambda, \mathbf{\Omega}) \approx \exp[-(1/\mu_0 + 1/\mu)\tau_{O_2}(\lambda; z_{top})] R_\lambda(\mathbf{\Omega}; \mathbf{\Omega}_0, \tau_c), \quad (4)$$

where we have already referred to $(1/\mu_0 + 1/\mu)$ as the airmass factor M in (3). The cloud layer's BRF, $R_\lambda(\mathbf{\Omega}; \mathbf{\Omega}_0, \tau_c)$, depends primarily on τ_c, also the scattering phase function $p_c(\theta_s)$, but only weakly in most (i.e., non-rainbow) directions, past its asymmetry factor

$$g = \int_0^\pi \cos(\theta_s) p_c(\theta_s) \sin(\theta_s) d\theta_s, \quad (5)$$

which is $\approx$0.85 for the liquid-water clouds considered in [7,8] and the present study. These cloud droplet properties vary little with λ between the A- and B-bands, let alone inside them.

Spectral dependence of $R_\lambda(\ldots)$ in (4) comes entirely from the absorbing gas inside the cloud, that is, $\left[\tau_{O_2}(\lambda; z)\right]_{z_{top}}^{z_{top}-H}$. However, estimation of cumulative path *inside the cloud* is a nontrivial question best framed in the time domain. See [21, and references therein] for investigations of cumulative path length in the framework of multiple scattering lidar, with active cloud remote sensing in mind at VNIR wavelengths. Just as for EPIC, a monostatic lidar system is in very nearly backscattering observation geometry, but the incidence is invariably quasi-normal to the cloud's upper boundary.

Imagine a short "pulse" of sunlight impinging on cloud top at time/path $ct = 0$. What is the distribution in time/path ct of the light emerging from the cloud? Let $R(ct, \mathbf{\Omega}; \mathbf{\Omega}_0, \tau_c)$ be that impulse response expressed in km^{-1}. Then, assuming uniform gaseous absorption coefficient k_λ in the cloud, one can compute the steady-

state absorption spectrum $R_\lambda(\mathbf{\Omega};\mathbf{\Omega}_0,\tau_c)$ from the so-called equivalence theorem [22, among others]:

$$R_\lambda(\mathbf{\Omega};\mathbf{\Omega}_0,\tau_c) \equiv \hat{R}(k_\lambda,\mathbf{\Omega};\mathbf{\Omega}_0,\tau_c) = \int_0^\infty \exp(-k_\lambda\, ct) R(ct,\mathbf{\Omega};\mathbf{\Omega}_0,\tau_c)\,\mathrm{d}ct, \tag{6}$$

which is simply the Laplace transform of $R(ct,\mathbf{\Omega};\mathbf{\Omega}_0,\tau_c)$ with k_λ being the Laplace conjugate variable of path length ct. Normalized by $\hat{R}(0,\mathbf{\Omega};\mathbf{\Omega}_0,\tau_c)=\int_0^\infty R(ct,\mathbf{\Omega};\mathbf{\Omega}_0,\tau_c)\mathrm{d}ct$, $R(ct,\mathbf{\Omega};\mathbf{\Omega}_0,\tau_c)$ becomes the probability density function (PDF) of the random variable ct. This path length distribution has a mean, variance, and so on. Higher moments are out-of-scope for the present study, but it is important to know the mean in-cloud cumulative path, i.e.,

$$\langle ct\rangle(\mathbf{\Omega};\mathbf{\Omega}_0,\tau_c) = \frac{\int_0^\infty ct\, R(ct,\mathbf{\Omega};\mathbf{\Omega}_0,\tau_c)\,\mathrm{d}ct}{\int_0^\infty R(ct,\mathbf{\Omega};\mathbf{\Omega}_0,\tau_c)\,\mathrm{d}ct} = \frac{-1}{\hat{R}(0,\mathbf{\Omega};\mathbf{\Omega}_0,\tau_c)}\left.\frac{\partial\hat{R}}{\partial k_\lambda}\right|_{k_\lambda=0}, \tag{7}$$

where the denominator $\hat{R}(0,\mathbf{\Omega};\mathbf{\Omega}_0,\tau_c)$ is the steady-state radiance in the continuum, i.e., near but outside the absorption band. A priori, $\langle ct\rangle(\mathbf{\Omega};\mathbf{\Omega}_0,\tau_c)$ is also a function of other basic cloud properties, such as physical thickness H, the SSA for cloud particles (assumed unity here), and the droplet scattering phase function $p_c(\theta_s)$.

Starting with some version of (7), $\langle ct\rangle(\mathbf{\Omega};\mathbf{\Omega}_0,\tau_c)$ has been derived in closed form for standard approximations in 1D RT in plane-parallel clouds:

- Asymptotic theory views opaque scattering plane-parallel media as a perturbation of a semi-infinite medium ($\tau_c\to\infty$); it leads to [23, p. 591]

  $$\langle ct\rangle(\mathbf{\Omega};\mathbf{\Omega}_0,\tau_c) \approx (\mu+\mu_0)H, \tag{8}$$

  for $\tau_c \gg 1$, when the SSA is unity (non-absorbing media) and $p_c(\theta_s)=1/4\pi$ (isotropic scattering).[1] Originally, this expression was derived for the mean *optical* path length $\Lambda=\sigma_c ct$: $\langle\Lambda\rangle \approx (\mu+\mu_0)\tau_c$, which is equal to the mean number of scatterings for radiance reflected from a uniform media [23, p. 584]. Multiplying both sides by the continuum mean-free-path (MFP), which is the inverse of extinction $\sigma_c^{-1}=H/\tau_c$, yields (8).
- In the diffusion approximation, focus is exclusively on the 0th and 1st spherical harmonics of the radiance field and of the scattering phase function, hence it will predict reflected flux, i.e., radiance escaping at TOA weighted by $|\Omega_z|$ and averaged over $\mathbf{\Omega}$ in the upwelling hemisphere:

  $$F_{\mathrm{TOA}}(\mathbf{\Omega}_0,\tau_c) = \int_{\Omega_z<0} I_{\mathrm{TOA}}(\mathbf{\Omega};\mathbf{\Omega}_0,\tau_c)|\Omega_z|\mathrm{d}\mathbf{\Omega}. \tag{9}$$

  For conservative (SSA = 1) scattering, this model leads to [21,24]

  $$\langle ct\rangle_F(\mathbf{\Omega}_0,\tau_c) = \frac{\int_{\Omega_z<0}\langle ct\rangle(\mathbf{\Omega};\mathbf{\Omega}_0,\tau_c) I_{\mathrm{TOA}}(\mathbf{\Omega};\mathbf{\Omega}_0,\tau_c)|\Omega_z|\mathrm{d}\mathbf{\Omega}}{F_{\mathrm{TOA}}(\mathbf{\Omega}_0,\tau_c)} \approx \left(\frac{2}{3}+\mu_0\right)H\times[1+C(\tau_c,g,\mu_0)], \tag{10}$$

  where $C(\tau_c,g,\mu_0)$ is a pre-asymptotic correction term that decays as $1/\tau_c$ at large values. Now, Ref. [24] provides only a partial derivation of (10) in its Appendix D, and [21] only provides $C(\tau_c,g,1)$, albeit with excellent Monte Carlo validation, in view of the multiple-scattering lidar focus. We therefore provide here, in Appendix A, the explicit expression for $C(\tau_c,g,\mu_0)$ and describe the main steps of its derivation.

Either way, we see that $\langle ct\rangle(\mathbf{\Omega},\mathbf{\Omega}_0,\tau_c)$ is, to leading order, proportional to physical cloud thickness H, irrespective of scattering details, and the proportionality factor depends only on illumination and viewing geometry.

If $\langle ct\rangle(\mathbf{\Omega},\mathbf{\Omega}_0,\tau_c)$ is all we know about $R(ct,\mathbf{\Omega};\mathbf{\Omega}_0,\tau_c)$, then our logical estimate of steady-state spectral radiance $R_\lambda(\mathbf{\Omega};\mathbf{\Omega}_0,\tau_c)$ is obtained by setting

$$R(ct,\mathbf{\Omega};\mathbf{\Omega}_0,\tau_c) = \hat{R}(0,\mathbf{\Omega};\mathbf{\Omega}_0,\tau_c)\,\delta[ct-\langle ct\rangle(\mathbf{\Omega};\mathbf{\Omega}_0,\tau_c)], \tag{11}$$

hence, from (6),

$$R_\lambda(\mathbf{\Omega};\mathbf{\Omega}_0,\tau_c) = \hat{R}(0,\mathbf{\Omega};\mathbf{\Omega}_0,\tau_c)\exp[-k_\lambda\langle ct\rangle(\mathbf{\Omega};\mathbf{\Omega}_0,\tau_c)], \tag{12}$$

where we can use the mean absorption coefficient in the cloud:

$$k_\lambda \approx [\tau_{\mathrm{O}_2}(\lambda;z)]_{z_{\mathrm{top}}}^{z_{\mathrm{top}}-H}/H. \tag{13}$$

We now ask: under what conditions is the above hypothesis that "all we know about the path length distribution is its mean" is likely to be good enough? It boils down to one or both of the following requirements. First, the width (e.g., standard deviation) of the PDF for ct could be relatively small with respect to its mean $\langle ct\rangle$. Second, the combined value of $k_\lambda ct$ may remain small enough over said width of the PDF of ct that one can invoke the 1st-order linear approximation for $\exp(-k_\lambda ct)\approx 1-k_\lambda ct$ in (6). In the case of optically thick clouds, the first condition is *not* expected to be verified; it has indeed been shown that, at least for reflected light, the variance of ct increases with COT, while $\langle ct\rangle$ does not, as COT increases without bound [e.g., 24, and references therein]. Best therefore to look into the second option where, because of the spectral integration discussed in the previous and following subsections, we should consider both ct and k_λ as random variables. Having just dismissed the PDF of ct as inherently broad for high-COT clouds, we are relieved that the variability of k_λ is overwhelmingly dominated by small values in both O_2 absorption bands (where, at the prevailing pressures and temperatures, the wings occupy more of the spectrum than the cores of absorption lines). Although it is out of the scope of the present study, a thorough examination of the assumption of a degenerate (i.e., Dirac-δ) PDF for ct is in order with O_2 absorption in mind, and additional reasons for this are articulated further on. At present, we will be content with the fact that, in spite of all the simplifying assumptions, the analytical forward model developed herein leads to identical conclusions about EPIC's A- and B-band information content for vertical cloud profiling as in the companion paper [7] where accurate spectral integration and 1D RT modeling was used—as a "black box"— to support a sophisticated statistical estimation approach.

We can now form the observed differential optical absorption spectroscopy (DOAS) ratio: applying (4), we have

$$r_\lambda(\mathbf{\Omega};\mathbf{\Omega}_0,\tau_c) = \frac{R_{\mathrm{TOA}}(\lambda\in\Delta\lambda)}{R_{\mathrm{TOA}}(\lambda\notin\Delta\lambda)} \approx \mathrm{e}^{-(1/\mu_0+1/\mu)\tau_{\mathrm{O}_2}(\lambda;z_{\mathrm{top}})}\frac{R_\lambda(\mathbf{\Omega};\mathbf{\Omega}_0,\tau_c)}{\hat{R}(0,\mathbf{\Omega};\mathbf{\Omega}_0,\tau_c)} = \mathrm{e}^{-\left[\left(\frac{1}{\mu_0}+\frac{1}{\mu}\right)\tau_{\mathrm{O}_2}(\lambda;z_{\mathrm{top}})+k_\lambda\langle ct\rangle(\mathbf{\Omega};\mathbf{\Omega}_0,\tau_c)\right]}, \tag{14}$$

where "$\lambda\in\Delta\lambda$" is shorthand for any wavelength inside the absorption band of interest, and conversely for "$\lambda\notin\Delta\lambda$" (although outside, it should be as near to the absorption band as possible so that scattering properties are almost identical for both wavelengths).

For $\langle ct\rangle(\mathbf{\Omega};\mathbf{\Omega}_0,\tau_c)$ in (14), we take the best of both predictive models in (8) and (10):

$$\langle ct\rangle(\mathbf{\Omega};\mathbf{\Omega}_0,\tau_c) \approx (\mu+\mu_0)H\times[1+C(\tau_c,g,\mu_0)]. \tag{15}$$

[1] Although van de Hulst [23] provides neither proof nor speculation, we confidently surmise that (8) holds for any phase function in the limit $\tau_c\gg 1/(1-g)$. This assertion is based on the fact that, in the diffusion approximation, g only appears in the pre-asymptotic correction term in (10).

Indeed, asymptotic theory provides the desirable angular reciprocity upfront in the prefactor of (8) while diffusion theory in (10) restores the anticipated weak dependence on COT and g at the cost of a minor violation of reciprocity confined to the pre-asymptotic correction term.

Invoking (12) and (13), the negative natural logarithm of the DOAS ratio in (14) and (15) is

$$-\log r_\lambda(\mathbf{\Omega};\mathbf{\Omega}_0,\tau_c) \approx (1/\mu_0+1/\mu)\tau_{O_2}(\lambda;z_{top}) + (\mu+\mu_0)[\tau_{O_2}(\lambda;z)]_{z_{top}-H}^{z_{top}} \times (1+C(\tau_c,g,\mu_0)), \quad (16)$$

which is a simplified monochromatic forward model for DOAS ratios. To get the required O_2 optical depths at or between arbitrary altitudes, we assume a simple exponential profile in atmospheric pressure, hence of O_2. Therefore, a first-order approximation for $\tau_{O_2}(\lambda;z)$ is $\tau_{O_2}(\lambda;0)$ times $e^{-z/H_{mol}}$, where we can set the pressure scale height H_{mol} to $\approx$8 km.

2.4. Absorption-band integration

We recall from Fig. 1 that the EPIC sensor is performing weighted spectral integrations over the A- and B-bands. For that, we introduce a new notation for (12):

$$R_{\Delta\lambda}(\mathbf{\Omega};\mathbf{\Omega}_0,\tau_c) = \hat{R}(0,\mathbf{\Omega};\mathbf{\Omega}_0,\tau_c)\int_{\Delta\lambda}\exp[-k_\lambda\langle ct\rangle(\mathbf{\Omega};\mathbf{\Omega}_0,\tau_c)]f_{in}^\star(\lambda)d\lambda, \quad (17)$$

where the broad spectral variability stems from (13). In view of (6), that means that there is actually a double integration going on, both in the spectral domain and over path lengths. The above "all-we-know-is-the-mean-path-length" assumption will be more accurate if the PDF of the random variable ct is skewed toward short paths where Beer's exponential transmission law is nearly linear in path length, at least for the smaller values of k_λ representative of the wings of the O_2 spectral lines. For light *reflected* by optically thick clouds, numerical simulations show that this is indeed the case, e.g., [24].

Similarly, the DOAS ratio observed by EPIC is a ratio of spectral integrals over (14). However, because scattering properties vary little in the continuum ($\lambda\notin\Delta\lambda$), one can formulate $r_{\Delta\lambda}(\mathbf{\Omega};\mathbf{\Omega}_0,\tau_c)$ simply as the in-band integration of $r_\lambda(\mathbf{\Omega};\mathbf{\Omega}_0,\tau_c)$ from (14). From there, taking logs, $\log r_{\Delta\lambda}(\mathbf{\Omega};\mathbf{\Omega}_0,\tau_c)$ will look like (16) but using the effective optical depth from (2) for both A- and B-bands.

To get the *effective* O_2 optical depths at or between arbitrary altitudes based on its sea-level value in (2), we can assume the same exponential profile as for $\tau_{O_2}(\lambda;z)$. Hence $\tau_{O_2}^{(\Delta\lambda)}(z) = \tau_{O_2}^{(\Delta\lambda)}(M)\exp(-z/H_{mol})$.

Fig. 3 shows the B- and A-band DOAS ratios $r_{\Delta\lambda}(\mathbf{\Omega}_0;\mathbf{\Omega}_0,\tau_c)$ from (16) for EPIC as functions of z_{top} and H in [km] when $\mu=\mu_0=2/3$, hence an intermediate airmass of 3, and (τ_c,g) = (30,0.85), scaled to (15,0.7), as explained in Appendix A, for improved accuracy of the diffusion approximation. We note the sensitivity in both bands to both cloud properties. Apparently, however, only the range of DOAS values seems to change, not the pattern of dependence on cloud parameters. Further on, we discuss the ramifications of this similarity—but not identity, due to the nonlinear dependence on $\tau_{O_2}^{(\Delta\lambda)}$ from (2).

To summarize our stance on spectral integration, by considering only the effective absorption optical thickness in (2), we have implicitly ignored the impacts of spectral correlations. Because transmission laws that account for spectral correlations tend to raise the value of transmission for a given path length, making it less exponential and more linear, we expect this future improvement will reinforce not only the robustness of the spectral integral but also the validity of our other key assumption in (11), namely, that all we know is the first moment of the path length within clouds.

3. Forward model bias estimation

Following [25], we can divide (16) by the known airmass factor $(1/\mu_0+1/\mu)$ in (3), and thus define implicitly the "apparent" or "centroid" cloud-top altitude $z_{top}^{(app)}$ in

$$\tau_{O_2}(\lambda;z_{top}^{(app)}) = \begin{cases} -\log r_\lambda^{(obs)}/(1/\mu_0+1/\mu) & \text{(observed)} \\ \tau_{O_2}(\lambda;z_{top}) + \mu\mu_0[\tau_{O_2}(\lambda;z)]_{z_{top}-H}^{z_{top}} & \\ \quad\times(1+C(\tau_c,g,\mu_0)) & \text{(modeled)} \end{cases} \quad (18)$$

as the inverse $z_\lambda(\tau_{O_2}) = \tau_{O_2}^{-1}(\lambda;\tau_{O_2})$ of the (monochromatic) map defined in (1) where the right-hand side is either modeled by setting z_{top} and H or obtained from a measurement $r_\lambda^{(obs)}$ of the DOAS ratio. This estimate of z_{top} is obviously going to be biased low as soon as $H>0$ by the second term that captures geometry-dependent in-cloud path length cumulation.

To see this, we invoke the exponential profile in O_2 optical depth with scale height H_{mol}. Then the lower equation for $z_{top}^{(app)}$ in (18) simplifies to

$$z_{top}^{(app)} \approx z_{top} - H_{mol}\log\left[1+\mu_0\mu\left(e^{H/H_{mol}}-1\right)\times(1+C(\tau_c,g,\mu_0))\right], \quad (19)$$

irrespective of λ or $\Delta\lambda$, i.e., whether using the A- or B-band (in this approximation). If, moreover, the cloud is geometrically thin in the sense that $H\ll H_{mol}$, then a 1st-order Taylor expansion leads to $z_{top}^{(app)} \approx z_{top} - \mu_0\mu H\times(1+C(\tau_c,g,\mu_0))$, now irrespective of H_{mol} as well.

For EPIC, we have $\mathbf{\Omega}\approx-\mathbf{\Omega}_0$, hence $\mu\approx\mu_0$. We then see in (19) that the expected negative bias is clearly at its greatest, for given H, at sub-solar observation geometry ($\mu=\mu_0=1$): $z_{top}^{(app)} \approx z_{top} - H\times(1+C(\tau_c,g,\mu_0))$. See Fig. 2 in [25] and Fig. 6 in [8] for qualitative confirmation on observational and computational grounds, respectively. In reality and in exact 1D RT, the maximum bias of predicted in (19) is a slight overestimation. Our Fig. 4 shows $z_{top}-z_{top}^{(app)}$ normalized to H from (19) with $\mu=\mu_0$ and H_{mol} = 8 km. We see that for oblique solar/view geometry, the bias is between 0 (at grazing sun/views) and H.

It is somewhat disconcerting that, in its final form (19), our simplified model has no explicit spectral dependence and, therefore, cannot be used to distinguish A- and B-band cloud information contents, irrespective of how the spectral band integration is modeled. We would normally expect that access to two wavelengths/bands would lead to a way of extracting both z_{top} and H, the parameters used here to define the cloud profile. Instead, they combine invariably into $z_{top}^{(app)}$ in (19).

Several approximations were made along the way, and the one where spectral dependence was all but lost is not immediately apparent. Careful scrutiny however leads back to the early step in (11) where *only the mean* path length was assumed known for the sunlight that entered the cloud and was eventually reflected back to space. This lead to a simple exponential dependence on *both* above-cloud and in-cloud absorption by O_2. If only two path length moments were known, e.g., mean and variance, then the in-cloud term $R_\lambda(\mathbf{\Omega};\mathbf{\Omega}_0,\tau_c)$ obtained from (6) would not be an exponential [26]. Consequently, the dependence on $\tau_{O_2}(\lambda;0)$ would not cancel out after the later—and quite reasonable—approximation that $\tau_{O_2}(\lambda;z)$ has the same exponential profile in z for all λ.

The insight gained here is that a diversity of path lengths in the scattering medium is crucial to the access to more than one cloud

parameter. One straightforward way of diversifying in-cloud path length, even with a single O_2 channel, is by varying view angle, i.e., μ in expression (19) for $z_{\rm top}^{\rm (app)}$. This is the option that was exercised by the POLDER/PARASOL mission, as previously mentioned in connection with [25,27], but it is not available for EPIC. The alternative, this one available for EPIC, is to have more than one spectral channel. However, the forward model needs more sophistication than used here, where the goals are only (*i*) to estimate CTH retrieval bias when in-cloud scattering is neglected, and (*ii*) to demonstrate that instrument error needs to be small enough to distinguish the spectral signals. Just how small in EPIC's A- and B-band case is the topic we now broach.

4. Impact of measurement error

The simplified DOAS ratio model in (16) can also be used to translate measurement error on $r_{\Delta\lambda}(\ldots)$ into uncertainty in the inferred $z_{\rm top}^{\rm (app)}$, which is obtained by inverting said model without the second (in-cloud path length) term, cf. (18) and (19). Taking differentials on both sides of (16), and using (1), we obtain

$$\begin{aligned}\frac{\delta r_\lambda}{r_\lambda} &\approx \Big[\Big(\frac{1}{\mu_0}+\frac{1}{\mu}\Big)k_\lambda(z_{\rm top})+(\mu+\mu_0\Big) \\ &\quad\times\big(k_\lambda(z_{\rm top}-H)-k_\lambda(z_{\rm top})\big)\Big]\,\delta z_{\rm top}^{\rm (app)} \\ &\approx (\mu_0+\mu)\Big[\Big(\frac{1}{\mu_0\mu}-1\Big)k_\lambda(z_{\rm top})+k_\lambda(z_{\rm top}-H)\Big]\,\delta z_{\rm top}^{\rm (app)},\end{aligned} \tag{20}$$

where, for simplicity, we have neglected the pre-asymptotic correction term that multiplies the term in $(\mu_0+\mu)$ in the upper expression. Invoking the approximately exponential profile of

$$k_\lambda(z)=-\frac{\rm d}{{\rm d}z}\tau_{O_2}(\lambda,z)\approx\frac{\tau_{O_2}(\lambda,0)}{H_{\rm mol}}\,\exp(-z/H_{\rm mol}), \tag{21}$$

the band-effective O_2 absorption optical depth at sea level in (2), hence symbolically λ becomes $\Delta\lambda$, and EPIC's viewing geometry $(\mu=\mu_0)$, we have

$$\begin{aligned}\frac{\delta r_{\Delta\lambda}}{r_{\Delta\lambda}} &\approx \frac{\tau_{O_2}^{(\Delta\lambda)}(2/\mu_0)}{H_{\rm mol}}2\mu_0\Big[\frac{1}{\mu_0^2}+{\rm e}^{H/H_{\rm mol}}-1\Big] \\ &\quad\times\exp\left(-z_{\rm top}/H_{\rm mol}\right)\delta z_{\rm top}^{\rm (app)}.\end{aligned} \tag{22}$$

As discussed in [7], a common assumption for the relative error in DOAS ratio, $\Delta r_\lambda/r_\lambda$, is 1 to 1.5%. This contrasts with the $\approx$3% error assumed for *absolute* radiometry, but some of that error (e.g., calibration drift) cancels in the ratio. Thus, setting the right-hand side of (22) to 0.015 (1.5%), and solving for $\delta z_{\rm top}^{\rm (app)}$, we obtain the following estimate of retrieval error:

$$\Delta z_{\rm top}^{\rm (app)}\approx\frac{0.015\,H_{\rm mol}}{\tau_{O_2}^{(\Delta\lambda)}}\times\frac{{\rm e}^{z_{\rm top}/H_{\rm mol}}}{2\mu_0\big(\mu_0^{-2}+{\rm e}^{H/H_{\rm mol}}-1\big)}, \tag{23}$$

where $H_{\rm mol}=8$ km. For specificity, we take an airmass factor of 5: $\mu_0=0.4$, $\theta_0\approx66°$, which is approaching the upper limit of 6 in Fig. 2, past which sphericity effects start to matter. With that assumption, hence $\tau_{O_2}^{(\Delta\lambda)}\approx0.33$ and 0.14 for A-band and B-band, respectively. This yields $\Delta z_{\rm top}^{\rm (app)}\approx0.14$ and 0.32 km, respectively for A- and B-band estimates for a low cloud layer, $(z_{\rm top},H)=(2.5,2)$ km. For the same cloud at a height of $\approx$8 km, we will have roughly ${\rm e}\approx2.7$ times larger uncertainties. At smaller (larger) airmasses, we will have somewhat larger (smaller) uncertainties, due to the decreased (increased) amounts of O_2 absorption. In the 1–4 km range, H has a minor role in (23) since ${\rm e}^{H/8}-1$ has to compete with $1/\mu_0^2$.

The joint $(z_{\rm top},H)$ retrieval method proposed by Yang et al. [8] uses two-entry look-up tables (LUTs) for those cloud parameters as a function of two observable quantities denoted $h_{\rm sum}$ and $h_{\rm diff}$, which are in essence the sum and difference of the estimates of $z_{\rm top}^{\rm (app)}$ for the A- and B-bands. These LUTs are displayed in Fig. 9 of [8] (reproduced as Fig. 6 in the companion paper [7]) for $\theta_0=40°$ and three different choices of τ_c. The ranges of $h_{\rm sum}$ go from $\approx$2 km to 20 km or more. In contrast, the full ranges of $h_{\rm diff}$ are only 0.18, 0.20, and 0.55 km, respectively for $\tau_c=30$, 10, and 5. In the joint retrieval, we would want to be able to locate the observation coordinate $(h_{\rm sum},h_{\rm diff})$ as precisely as possible to infer $(z_{\rm top},H)$ accurately. To be quantitative, we would want the measurement uncertainties (error bars) on $(h_{\rm sum},h_{\rm diff})$ to be, say, 5-to-10 times smaller than the overall range of the relevant LUT. For $h_{\rm diff}$ that translates to an uncertainty (quantified by, e.g., "2 sigmas") no larger than $\approx$0.05 km.

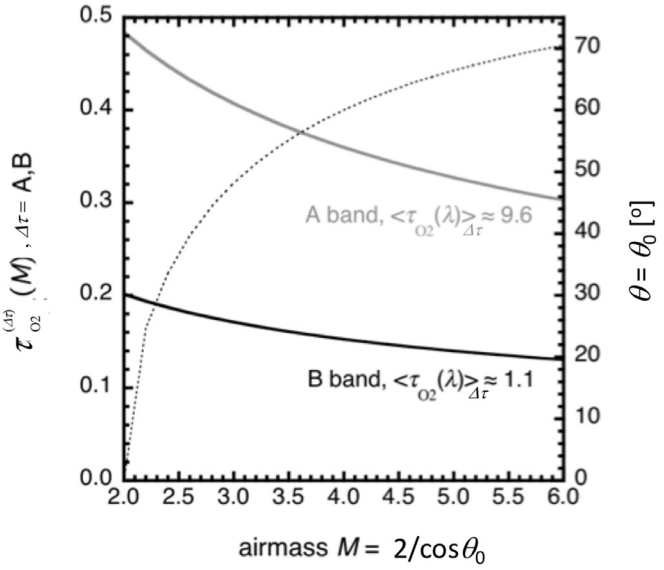

Fig. 2. Plots of $\tau_{O_2}^{(\Delta\lambda)}(M)$ in (2) and (3) for A- and B-bands, with a reminder of the far more different filter-averaged $\tau_{O_2}(\lambda)$, and correspondence between M and θ_0 for EPIC.

We can now bring to bear the estimate of uncertainty on retrieved centroid cloud top height $z_{\rm top}^{\rm (app)}$ in (23). The resulting uncertainty on $h_{\rm sum}$ and $h_{\rm diff}$ is the root-mean-square (RMS) sum of $\Delta z_{\rm top}^{\rm (app)}$ for the A- and B-bands. Fig. 5 shows the outcome (i.e., "1 sigma") expressed in km. We clearly see that these sensor-induced uncertainties may be very reasonable for the horizontal axes ($h_{\rm sum}$) in Fig. 9 of [8], better still, if divided by $\sqrt{2}$ (i.e., the estimate of the uncertainty on the mean of $z_{\rm top}^{\rm (app)}$ for the A- and B-bands. However, the numbers in Fig. 5, especially if doubled to estimate the "2 sigma" range, will overwhelm the full extent of the vertical axes ($h_{\rm diff}$) of [8]'s Fig. 9. This is in spite of the undeniable sensitivity of $h_{\rm diff}$ to H in the LUTs.

Conversely, to reduce uncertainty on $z_{\rm top}^{\rm (app)}$ enough to fit 5-to-10 observed "points" into the vertical axes of [8]'s Fig. 9, we would need to reduce the ranges obtained in our Fig. 5 to values no larger than $\approx$0.025 km, i.e., 10-to-20 times smaller. That would require relative uncertainties on the DOAS ratios to be 10-to-20 times smaller than 1.5%, which is not feasible with current or foreseeably futuristic space-based sensors.

5. Closing remarks

5.1. Summary

By invoking the signal physics underlaying EPIC's differential optical absorption spectroscopic (DOAS) ratios for the A- and B-bands, we have shown that these two measurements are too re-

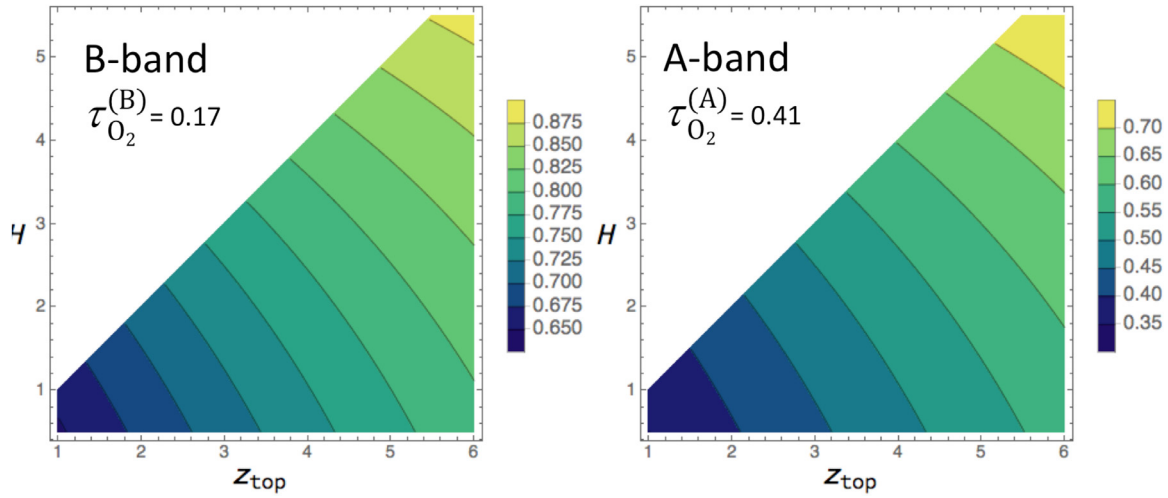

Fig. 3. DOAS ratios for EPIC's B- (left) and A-band (right) as functions of the two cloud properties of interest: CTH z_{top} and CGT H, both in [km]. Other parameters are provided in main text.

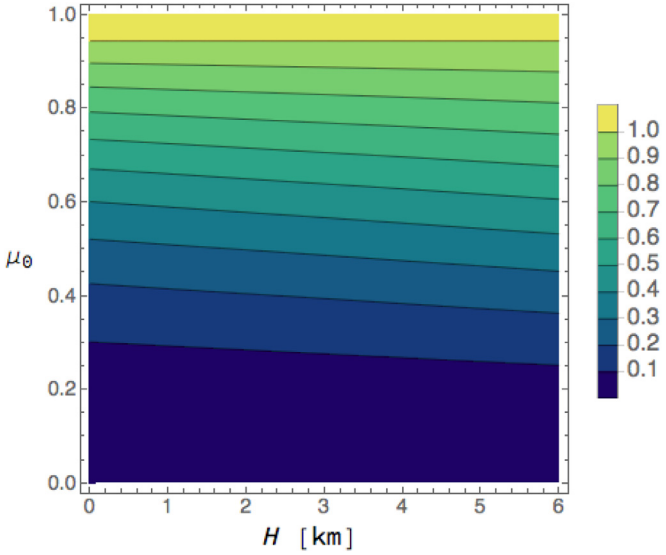

Fig. 4. Normalized CTH bias $\left(z_{top} - z_{top}^{(app)}\right)/H$ from (19) for EPIC's solar/viewing geometry ($\mu_0 = \mu$), and $H_{mol} = 8$ km.

dundant to allow for retrieving both cloud top height (CTH) and cloud geometrical thickness (CGT). In the absence of any independent knowledge of CTH, this important cloud property can be inferred from either or, better, both A- and B-band channels (adopting the average, weighted as needed). However, if CGT is neglected altogether, these estimates will be biased low due to the O_2 absorption path length cumulated inside the cloud. A bias-correction scheme is in order, and a reasonable approach used by others assumes an adiabatic lapse rate to relate CTH and cloud base height (i.e., CTH minus CGT). This finding is consistent with the outcome of the investigation by Xu et al. [28] of dust plume height retrieval using EPIC's A- and B-band channels.

The above conclusion is also completely aligned with that of the companion paper [7] by the same authors as here along with others in the same journal where the statistical formalism of optimal estimation was used. The two-pronged research described in the present pair of articles builds on a preliminary investigation by Yang et al. [8] of EPIC's A- and B-band cloud sensing capability prior to DSCOVR's launch to the L_1 point, where the possibility of a joint retrieval of CTH and CGT was envisioned with an idealized instrument. Taking into account realistic levels of sensor noise makes it clear that only a robust retrieval of CTH should be targeted, and that is already a major contribution to cloud science for years to come.

5.2. A remarkable invariance property of mean path length

Before closing, we take note of a very interesting development in the optics of purely scattering media that relates directly to our present work with clouds and di-oxygen absorption, to diffuse optical tomography [29] in biomedical imaging [30], and to many other applications. Using thermodynamical and weak light absorption arguments Blanco and Fournier [31] showed theoretically that, in our notations,

$$\langle ct \rangle_F^{(all)} = 4V/S, \tag{24}$$

where:

- the superscript "(all)" means isotropic (Lambertian) illumination of the whole surface of the arbitrarily-shaped medium M, and we recall that the subscript "F" means integration over all escape angles to obtain hemispherical flux, in this case, perpendicular to the local outgoing normal, and averaging covers the whole boundary ∂M of the medium;
- V is the volume of M;
- S is the surface of M.

Surprisingly, the result does not depend on the details of the scattering phase function, nor on the opacity of the medium: it can be void of scatterers (i.e., the uniform extinction coefficient σ vanishes, hence only ballistic trajectories occur); or it can be very opaque ($\sigma V/S \gg 1$); or anything in between. This mean path invariance property was extended by Pierrat et al. to multiple scattering theory using both physical optics and time-dependent 3D radiative transfer [32]. Recently, Savo et al. [33] demonstrated its experimental validity in the laboratory.

In our present study, we use plane-parallel media that can be viewed, e.g., as rectangular parallelepipeds of height H and square horizontal section of side $L \gg H$. We then have $V = HL^2$ and $S = 2L^2 + 4HL$, hence $4V/S = 2H/(1 + 2H/L)$ and $\lim_{L\to\infty} 4V/S = 2H$ is the corresponding prediction for

$$\langle ct \rangle_F^{(all)} = R\langle ct \rangle_R + T\langle ct \rangle_T, \tag{25}$$

where $R \lesssim 1$ is the optically thick cloud's reflectivity, and $T = 1 - R \ll 1$ is its transmittivity, $\langle ct \rangle_R$ is the mean path for reflected light

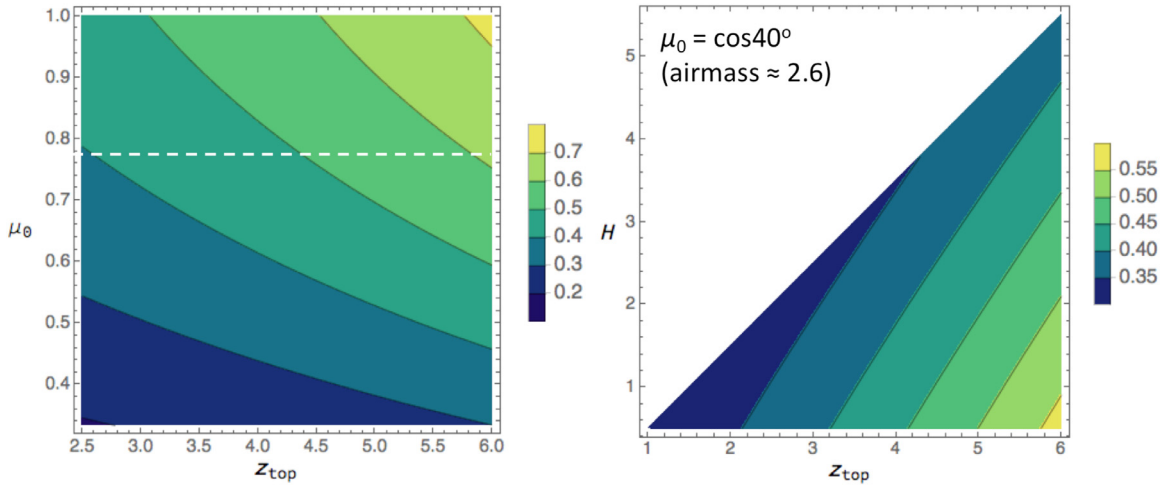

Fig. 5. Estimated uncertainties on h_{sum} or h_{diff} in Fig. 9 of [8]—equivalently, Fig. 6 of [7]—induced by instrumental error, modeled as the RMS sum of uncertainties on cloud centroid heights from the A- and B-bands. *Left:* Dependence on μ_0 in safe zone ($\gtrsim 1/3$) for sphericity effects, and on z_{top} in km when $H = 2$ km ($\mu_0 = \cos 40^\circ$ highlighted), using $\tau_{O_2}^{(\Delta\lambda)}(5)$ values from Fig. 2. *Right:* Dependence on H in km and $z_{top} \geq H + 0.5$ when $\mu_0 = \cos 40^\circ$ (as in [8]).

(any direction), denoted $\langle ct\rangle_F$ in the main text, and $\langle ct\rangle_T$ is its counterpart for transmitted light. With R approaching unity, hence vanishingly small T, our estimates of $\langle ct\rangle_R$ in (8) and in (10), after averaging over μ_0 (leading term only in the latter case) and over μ (in the former case), fall significantly short of $2H$. Although, they at least have the linear dependance H, and none on any other cloud optical property to first order. Consequently, $\langle ct\rangle_T$ in (25) must be large enough compared to H to compensate for the diminutive T in the weighted average. Appendix B draws on previously published results akin to the ones derived and used herein to show that (24) is indeed verified for light diffusing through plane-parallel slabs. To the best of our knowledge, therein is the first proof of the mean path length invariance property in (24) that uses formal diffusion theory.

5.3. Outlook

Future work will focus, on the one hand, on supporting the operational implementation of an algorithm to obtain CTH from EPIC's A- and B-bands using an informed guess for CGT to minimize retrieval bias; uncertainty on the retrieved CTH will be reduced by using both oxygen bands, and stated as part of the retrieval. On the other hand, we will be investigating applications of (24) to remote sensing and radiant energy budget estimation.

Acknowledgments

This research was carried out at the Jet Propulsion Laboratory, California Institute of Technology, under a contract with the National Aeronautics and Space Administration (NASA). ABD, QM and YY acknowledge partial financial support from NASA's ROSES program element for DSCOVR Earth Science Algorithms managed by Dr. Richard Eckman. AM is supported by the NASA/GSFC DSCOVR mission funded by NASA Earth Science Division. ABD acknowledges support from the MEASURES project at JPL managed by Dr. Joshua K. Willis. NF acknowledges financial support from CNES, Université de Lille and Région Haut-de-France. Moreover, part of the discussion and work between authors has been made possible through support from the Programme National de Télédétection Spatiale (PNTS, http://www.insu.cnrs.fr/pnts), under grant #PNTS-2017-04.

We thank Jay Herman, Marine Desmons, François Thieuleux, Jérôme Riédi, Céline Cornet, Philippe Dubuisson, Claudine Vanbauce, Frédéric Parol, Klaus Pfeilsticker, Alex Kokhanovsky, Lee Harrison, Ralf Bennartz, Denis O'Brien, Graeme Stephens, Suniti Sanghavi, Mark Richardson, Dave Crisp, Feng Xu, Sid Redner, and others for many fruitful discussions on probing clouds with the O_2 A-band. We thank Stéphane Blanco, Richard Fournier in particular for very interesting and stimulating discussions on the invariance property of mean path length for diffusion random walk. Finally, penetrating commentary by the anonymous reviewers of this manuscript was highly appreciated.

Appendix A. Prediction of mean in-cloud pathlength $\langle ct\rangle$ in the diffusion limit

A.1. Problem

We need an explicit expression for mean in-cloud pathlength $\langle ct\rangle$ as a function of cloud properties, namely, CGT H, COT τ, phase function asymmetry factor g, when the solar beam is either normal or oblique, which we represent with $\mu_0 = \cos SZA$.

In the diffusion approximation, we limit the spherical harmonic expansion of the time/path-dependent diffuse radiance field $I(ct, z, \mathbf{\Omega})$ to the 0^{th}- and 1^{st}-order terms. In plane-parallel geometry (hence 1D RT), letting $\mu = \Omega_z$, we have:

$$I(ct, z, \mathbf{\Omega}) = \frac{J(ct, z) + 3\mu F(ct, z)}{4\pi}, \tag{A.1}$$

irrespective of the azimuthal angle, where $J(ct, z)$ is the scalar (a.k.a. actinic) flux and $F(ct, z)$ the net vertical vector flux. Note that $J(ct, z)$ is closely related to the mean (directionally-averaged) radiance $J(ct, z)/(4\pi)$ and radiant energy density

$$U(t, z) = J(ct, z)/c.$$

The phase function expansion in spherical harmonics is similarly truncated:

$$p(\mu_s) = \frac{1 + 3g\mu_s}{4\pi}, \tag{A.2}$$

where $\mu_s = \mathbf{\Omega} \cdot \mathbf{\Omega}'$ is the cosine of the scattering angle, and g is its mean value, viewing $p(\mu_s)$ as a probability distribution; see (5) in main text. Note that $\mu_{(s)}$ in (A.1) and (A.2) is simply the 1st-order Legendre polynomial while $F(ct, z)$ and g are its respective coefficients in the two expansions.

Substitution of these truncated expansions in spherical harmonics into the time-dependent 1D RT equation leads to two coupled partial differential equations (PDEs); see, e.g., [24]. First, we have

the *exact* "continuity" equation that expresses the conservation of radiant energy:

$$\frac{\partial J}{\partial ct}+\frac{\partial F}{\partial z}=-\sigma_a J+q_J,\ \text{with } q_J(ct,z)$$
$$=F_0\sigma_s e^{-(\sigma_s+\sigma_a)z/\mu_0}\delta(ct-z/\mu_0), \quad (A.3)$$

where $\sigma_{s/a}$ is the scattering/absorption coefficient and F_0 is the time-integrated incoming irradiance. Second, we have the *approximate* "constituent" equation that expresses how the radiant energy density flow (net flux) is driven by the gradient in its density:

$$\frac{\partial F}{\partial ct}+\frac{1}{3}\frac{\partial J}{\partial z}=-((1-g)\sigma_s+\sigma_a)F+q_F,\ \text{with } q_F(ct,z)$$
$$=F_0\mu_0 g\sigma_s e^{-(\sigma_s+\sigma_a)z/\mu_0}\delta(ct-z/\mu_0). \quad (A.4)$$

Remark. Neglecting $\partial F/\partial ct$ in the above, as is usual in the time - dependent diffusion approximation per se, and noting that $q_F(ct, z)$ vanishes far from sources, we recognize

$$D=c/3((1-g)\sigma_s+\sigma_a)$$

as the diffusion coefficient in Fick's law:

$$F=-D\,\partial U/\partial z.$$

Substituting Fick's law into the continuity Eq. (A.3) with no absorption ($\sigma_a=0$) and, again, far from sources ($q_J\approx 0$), yields the classic parabolic PDE for diffusion processes such as heat transfer:

$$\left[\partial/\partial t-D(\partial/\partial z)^2\right]U=0.$$

Now, *not* neglecting $\partial F/\partial ct$ leads to the so-called "telegrapher's PDEs," which is a more accurate representation of the original linear transport problem than the diffusion approximation, especially at early times (short paths) [34], and that is the course we keep in the following.

The source terms $q_J(ct, z)$ and $q_F(ct, z)$ specified in the above PDEs model a *pulsed* version of solar irradiance impinging on the plane-parallel optical medium at $ct=z=0$. As in the main text, we will not consider absorption by the scattering particles (water does not absorb much at the O_2 A- and B-band wavelengths), hence $\sigma_a=0$ and the (total) extinction coefficient is $\sigma=\sigma_s$.

The required boundary conditions (BCs) express that no diffuse radiation is entering the plane-parallel medium at its top ($z=0$), nor at its base ($z=H$), at any time past the instant the pulse arrives at the upper boundary. Rephrasing this as a statement for incoming hemispherical fluxes, and going back to (A.1), these BCs can be expressed simply as:

$$J(ct,0)+2F(ct,0)=0, \quad (A.5)$$

$$J(ct,H)-2F(ct,H)=0, \quad (A.6)$$

for all $ct>0$.

For A- and B-band studies it is legitimate to neglect cloud droplet absorption: (σ_s,σ_a) becomes $(\sigma, 0)$. In that context, we can take Laplace transforms of (A.3)–(A.6), recalling from (6) that the Laplace conjugate variable of path ct is gaseous absorption k, and this leads to an equivalent steady-state problem expressed with coupled ordinary differential questions (ODEs):

$$k\hat{J}+\frac{d\hat{F}}{dz}=\hat{q}_J, \quad (A.7)$$

$$k\hat{F}+\frac{1}{3}\frac{d\hat{J}}{dz}=-(1-g)\sigma\hat{F}+\hat{q}_F. \quad (A.8)$$

To complement these coupled ODEs, Laplace-transformed BCs in (A.5) and (A.6) are:

$$\hat{J}(k,0)+2\hat{F}(k,0)=0, \quad (A.9)$$

$$\hat{J}(k,H)-2\hat{F}(k,H)=0. \quad (A.10)$$

This completes the definition of the boundary-value problem to solve.

A.2. Solution

Standard methods can be used to solve the above problem of coupled 1st-order ODEs. In the present study, however, we are not interested in the solution $[J, F](k, z)$ everywhere. Specifically, we require reflected flux at $z=0$, which is $\hat{J}(k,0)-2\hat{F}(k,0)]/4=\hat{J}(k,0)/2$, using the upper BC in (A.9). Normalized by the incoming downwelling flux, we obtain the cloud's reflectivity:

$$\hat{R}(k)=\frac{\hat{J}(k,0)/2}{\mu_0 F_0}. \quad (A.11)$$

This partial answer to our question about $\langle ct\rangle$ is given explicitly in [24] as a complicated function of four variables (kH, τ, g, μ_0) where σ and H have been combined into the (non-dimensional) COT, $\tau=\sigma H$ (denoted τ_c in the main text), and we note that k and H always occur as a non-dimensional product.

Although it can be done in closed form [35], we will not need to compute here the inverse Laplace transform of $\hat{R}(k,\ldots)$ to obtain $R(ct,\ldots)$. The last step to obtain $\langle ct\rangle$ is to expand *A*.11 into a 1st-order Taylor series in k:

$$\hat{R}(k,\ldots)=\hat{R}(0)+d\hat{R}/dk\big|_{k=0}k+\mathcal{O}(k^2). \quad (A.12)$$

Finally, we invoke (7) from the main text, which is a consequence of the fundamental equivalence relation in (6). In short, we have:

$$\langle ct\rangle_F(\cdots)=-\frac{1}{\hat{R}(0)}\left.\frac{d\hat{R}}{dk}\right|_{k=0}=-\frac{H}{\hat{R}(0)}\left.\frac{d\hat{R}}{dkH}\right|_{kH=0}. \quad (A.13)$$

The outcome, using $\hat{R}(kH,\tau,g,\mu_0)$ from Davis et al. [24], is thus the product of H and a complicated non-dimensional function of (τ, g, μ_0). Basically, we are looking at a rational function in multiple variables with additional polynomials multiplying $\exp(-\tau/\mu_0)$ in both numerator and denominator.

A.3. Result

The mean path length in (A.13) for cloud-reflected light in non-dimensionalized form is $\langle ct\rangle_F/H$, which remains a function of (τ, g, μ_0). Then, taking a cue from (10) in the main text, we can write it as $(2/3+\mu_0)\times[1+C(\tau,g,\mu_0)]$. We have thus identified explicitly the leading term for $\langle ct\rangle_F$ when $\tau\to\infty$, namely, $(2/3+\mu_0)H$. The pre-asymptotic correction term is then isolated, and it reduces to the following expression:

$$C(\tau,g,\mu_0)=\frac{p_0(\tau,g,\mu_0)-p_1(\tau,g,\mu_0)e^{-\frac{\tau}{\mu_0}}}{2\tau\mu_0(2+3\mu_0)(4+3(1-g)\tau)\left(3(1-g)\tau+(2-3\mu_0)\left(1-e^{-\frac{\tau}{\mu_0}}\right)\right)},$$

where (A.14)

$$p_0(\tau,g,\mu_0)=24\mu_0\left(1-3\mu_0^2\right)(-2+3(1-g)\mu_0)$$
$$+2\mu_0\left(44-54g-9(2-3g(2-g))\mu_0\right.$$
$$\left.-18(7-9g)\mu_0^2+81(1-g)^2\mu_0^3\right)$$
$$\times\tau+18\mu_0\left(3+2\mu_0(1-3\mu_0)-g\left(3-9\mu_0^2\right)\right)$$
$$\times(1-g)\tau^2, \quad (A.15)$$

and

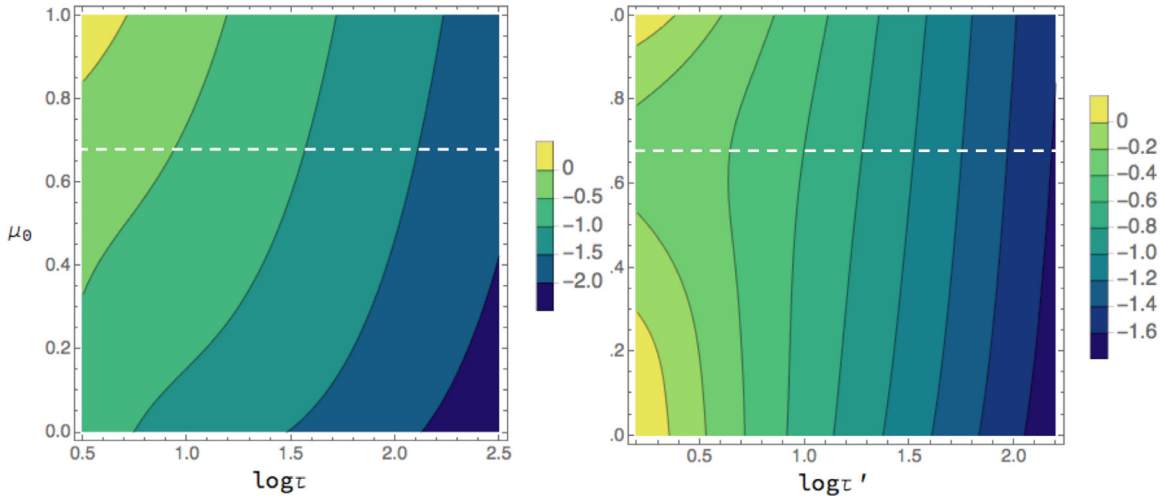

Fig. A.1. *Left:* $\log_{10}C(\tau, g, \mu_0)$ as function of $(\log_{10}\tau, \mu_0)$ for $g = 0.85$, with $\mu_0 = \frac{2}{3}$ highlighted since it is often used in the main text as a typical solar/viewing geometry for EPIC. *Right:* Same as left panel but using δ-Eddington rescaling [36], that is, to use $g' = (g - 0.5)/(1 - 0.5) = 0.7$ and $\log_{10}\tau' = \log_{10}\tau + \log_{10}0.5$.

$$\begin{aligned} p_1(\tau, g, \mu_0) = {} & 24\mu_0\big(1 - 3\mu_0^2\big)(2 - 3(1 - g)\mu_0) \\ & + 2\big(24 + \mu_0\big(8 - 18g - 9(10 - 3(2 - g)g)\mu_0 \\ & - 18(1 - 3g)\mu_0^2 + 81(1 - g)^2\mu_0^3\big)\big)\tau \\ & + 6(2 - 3\mu_0)(3 + (4 - 3\mu_0)\mu_0)(1 - g)\tau^2 \\ & + 9\mu_0(2 - 3\mu_0)(1 - g)^2\tau^3. \end{aligned} \tag{A.16}$$

Fig. A.1 shows $\log_{10}C(\tau, g, \mu_0)$ as a function of $\log_{10}\tau$ and μ_0 when $g = 0.85$, the canonical value for liquid water clouds, in the l-h panel. In the r-h panel, the same function is plotted, but for scaled cloud properties using the so-called δ-Eddington scheme [36]: (τ, g) becomes $(\tau', g') = ((1 - f)\tau, (g - f)/(1 - f))$, with $f = 0.5$. The rationale for this rescaling is that the accuracy of the present diffusion-type approximation is improved dramatically, especially at low τ, by removing the $\approx$50% of the single-scattered light that goes into the forward peak of the phase function and putting it back into the non-scattered beam, and then recomputing the asymmetry factor as g' to ensure that $(1 - g')\tau' = (1 - g)\tau$.

We note, finally, that the denominator in (A.14) is a 3rd-order polynomial in τ while $p_0(\tau, g, \mu_0)$ is only 2nd-order, hence a slow decay of $C(\tau, g, \mu_0)$ in $1/(1 - g)\tau$ with a prefactor given by

$$\begin{aligned} \lim_{\tau\to\infty}(1 - g)\tau \times C(\tau, g, \mu_0) = {} & (1 - g)\left(2 - \frac{1}{2 + 3\mu_0}\right) \\ & - (2 - 3g)\mu_0, \end{aligned} \tag{A.17}$$

which is plotted and discussed in Fig. A.2. We can clearly see the decay in τ^{-1} as τ increases without bound in Fig. A.1.

A4. Verification & validation

For a Monte Carlo solution of the time-dependent 1D RT equation for the light pulse starting at cloud top under normal incidence (μ_0 is unity), we refer to the Davis [21, Fig. 2]. Agreement with the diffusion approximation on the predicted values of $\langle ct\rangle_F/H$ is excellent over a large range of τ and two relevant values of g. Moreover, that is in spite of neglecting the time-derivative in (A.4), i.e., using bone fide time-dependent diffusion theory, not the improvement afforded by using the telegrapher's equations solved here.

This is tantamount to a *validation* of the diffusion-type approximations used here because validation is about "solving the right equations" [37]. Therefore, a model such as time-dependent 1D RT (implemented numerically with a Monte Carlo scheme) that is inherently more realistic than diffusion can provide validation data for a diffusion model. That is of course pending its own validation based on confrontation with real-world observations, even if they are laboratory-controlled instantiations of plane-parallel optical media [38].

Another check that is more qualitative, but brings more physical insight, is to show that $\langle ct\rangle_F \propto H$ follows from random walk theory, including the fact that dependencies on other cloud properties (τ, g) will at best be weak. Since we are now invoking a model that has less fidelity than our ODE-based model, we can only describe this exercise as a preliminary form of *verification*, which has been defined as "solving the equations right" [37].

We start by recalling that the space-time Green function $G(t, \mathbf{x})$ of the above-mentioned diffusion problem in the absence of boundaries is the solution of $\partial_t - D\nabla^2 = \delta(t)\delta(\mathbf{x})$. It's expression for $t > 0$ is $\exp(-\mathbf{x}^2/4Dt)/(\pi 4Dt)^{3/2}$. From there, two useful relations follow.

First comes, by integration, the well-known law of diffusion:

$$\int_{\mathbb{R}^3}\mathbf{x}^2 G(t, \mathbf{x})\mathrm{d}\mathbf{x} = \langle\mathbf{x}^2\rangle = 6Dt. \tag{A.18}$$

We recall here that $D = c\ell_t/3$, with $\ell_t = 1/(1 - g)\sigma$ being the so-called "transport mean-free-path," that is, the cumulative distance covered on average before the memory of the original direction has been all but erased in spite of the forward scattering tendency. It is the mean length of each step in an equivalent isotropic random walk, as is implicit in the diffusion model.

Second is the lesser known "law of first return," which answers the question: What is the probability $p_{1st}(t)\mathrm{d}t$ of a random walk returning to its plane of origin between time t and $t + \mathrm{d}t$? It can be shown [39,40] that

$$p_{1st}(t)\mathrm{d}t = \frac{c}{\sqrt{\pi}\,\ell_t}\left(\frac{\ell_t}{ct}\right)^{3/2}\exp(-\ell_t/2ct), \tag{A.19}$$

equivalently, $p_{1st}(ct) = p_{1st}(t)/c$. This PDF has a sharp increase from 0 at short times/paths, thanks to the exponential term, a peak at $ct = \ell_t/\sqrt{3}$, and a very long tail, decaying in $ct^{-3/2}$. In particular, both the mean and variance of ct are divergent. Physically, a pulse of light entering a semi-infinite scattering medium will keep coming back for a very long time due to the multiple scattering that sends it very deep in the absence of any absorption.

What happens it the medium has a finite geometric thickness ($H < \infty$), but also a very large optical thickness, even scaled for the forward scattering tendency? In other words, $\tau_t = (1 - g)\tau = H/\ell_t \gg 1$.

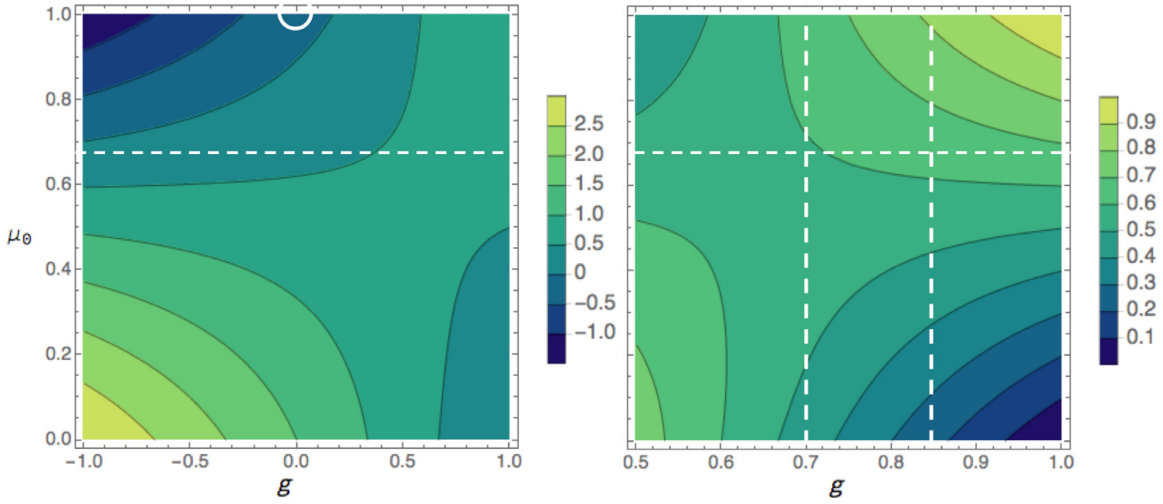

Fig. A.2. *Left:* The prefactor (A.17) of the slow decay of $C(\tau, g, \mu_0)$ in $1/(1-g)\tau$ is plotted versus (g, μ_0) over their full ranges, noting that $g<0$ is associated with *backward*-peaked phased functions. The value at (0,1) for isotropic scattering and normal incidence is highlighted, and it results in a slightly negative prefactor in (10), that is, a pre-asymptotic approach to (15) from below rather than from above. This is consistent with the trend displayed in [23, p. 590, Fig. 17.8] where the case of $\mu = \mu_0 = 1$ is studied for isotropic ($g = 0$) scattering. *Right:* Zoom of the l-h panel into the region where $0.5 < g < 1$; specific ranges for $g = 0.85$ and $g = 0.7$ are highlighted, corresponding respectively to the standard value of g for warm clouds and its (δ-Eddington) rescaled counterpart for $f = 0$. We note that the latter case has a narrow range of prefactor values, as it is close to the saddle point of the function of two variables. In both panels, the typical value of $\mu_0 = 2/3$ (used in the main text) is highlighted.

Basically, there is a characteristic time/path ct_H that the light takes to reach the cloud base in a substantial amount vis-à-vis the sum total of transmitted light. From (A.18), we can estimate it intuitively as[2] $ct_H \approx cH^2/6D = H^2/2\ell_t = H\tau_t/2$, which is $\gg H$ and thus $\ggg \ell_t$. That characteristic time/path acts in essence as a truncation for the heavy tail of $p_{1st}(ct)$ in (A.19). We thus seek the mean $\langle ct\rangle_F(H)$ of this truncated PDF: $p_H(ct) \approx p_{1st}(ct)$ if $ct < ct_H$, and 0 otherwise. That mean path can be estimated as $\langle ct\rangle_F(H) = \int_0^\infty ct\, p_H(ct)dct \approx \pi^{-1/2}\int_0^{ct_H} ct\,(ct/\ell_t)^{-3/2}dct/\ell_t$, ignoring the exponential "build-up" term. This leads to $\langle ct\rangle_F(H) \approx (\ell_t/\sqrt{\pi})\big[\sqrt{x}\big]_{x=0}^{ct_H/\ell_t}/(\frac{1}{2})$, where $ct_H/\ell_t = (\frac{1}{2})(H/\ell_t)^2$, which is indeed $\ggg 1$ since H/ℓ_t is already $\gg 1$ in the diffusion limit. Therefore, $\langle ct\rangle_F(H) \approx \sqrt{2/\pi}\,H$, irrespective of the other length-scale in the problem, namely, ℓ_t that, in turn, is determined by τ and g (along with H). In spite of all the approximations, even the prefactor, $\sqrt{2/\pi} \approx 0.8$, is not far from the proper hemispherical average of $(\mu + \mu_0)$, which is unity (hemispherical averages of μ_0 and μ contribute each 1/2).

In summary, continuous-time random walk theory explains why $\langle ct\rangle_F \propto$(and even $\approx$)H for optically thick clouds, irrespective of τ and g.

Appendix B. Verification of mean path invariance for diffuse propagation through plane-parallel slabs

In §5 we noted that a remarkable invariance property expressed in (24) was recently uncovered for the mean path length $\langle ct\rangle_F^{(all)}$ that corresponds to isotropic irradiance uniformly distributed over every boundary point of the uniform but arbitrarily-shaped optical medium M, as well as directionally-integrating sensors covering the boundary ∂M. What is truly remarkable about the result is that it holds independently of the opacity. It can even be void of scattering particles, and all trajectories are ballistic. If not, then their density is immaterial, as is their phase function, as long as their is no absorption (i.e., conservative scattering, SSA is unity).

What makes the fact that $\langle ct\rangle_F^{(all)}$ is invariably four times the volume V of M divided by its surface S relevant to our study is that, by definition, "reflected" light comes from the illuminated surfaces of the medium [42]. So, in this case, all the light is reflected, even if it originated on the opposite side of the medium. A key element of the present study is that the mean path length for light reflected from a plane-parallel slab is proportional to its geometrical thickness H. What is V/S, if not a generalization of H (actually $H/2$) to arbitrary cloud geometry?

We noted in (25) that for a plane-parallel slab, $\langle ct\rangle_F^{(all)}$ is a weighted sum of the mean paths for reflected and transmitted light. However, we also noted that our present diffusion-theoretical estimates of $\langle ct\rangle_R$ for the reflected light, which for the optically thick media amenable to the diffusion approximation are the most heavily weighted, fall short of the expected $2H$ from the invariance rule, even after the required angular integration (hemispherical averages of μ_0 and, as needed, μ are 1/2).

Here, we revisit some previous work [43,44] on path length statistics for both reflected and transmitted light in the diffusion limit. However, in contrast with App. A, *isotropic* illumination is used rather than a *collimated* incoming beam, which is consistent with the set-up for the invariant mean path length result in (24).

B.1. Reflection

Davis et al. [43] formulated the concept of "off-beam," or "multiple-scattering," or "wide-field-of-view" lidar as a novel tool for cloud remote sensing, specifically targeting H and τ_c.

One goal is to obtain τ_c without requiring absolute radiometric calibration nor loss of sensitivity at large optical thickness. The loss of sensitivity to τ_c can be clearly seen, e.g., in the well-known two-steam/diffusion expression for the albedo of a plane-parallel cloud:

$$R(\tau_t) = \frac{\tau_t}{2\chi + \tau_t}, \tag{B.1}$$

where $\tau_t = H/\ell_t = (1-g)\tau_c$ is the scaled optical thickness and χ is the so-called "extrapolation scale" expressed in units of the transport mean-free-path $\ell_t = 1/(1-g)\sigma$, which was used extensively in §A.4 on the approach to $\langle ct\rangle_R$ via random walk statistics rather than PDEs and numerical simulation (generally with Monte Carlo techniques). The numerical value of χ is determined by comparison with a more accurate representation of the transport problem at hand.

[2] In solid-state physics, $2t_H = H^2/c\ell_t$ is known as the Thouless dwell time [41].

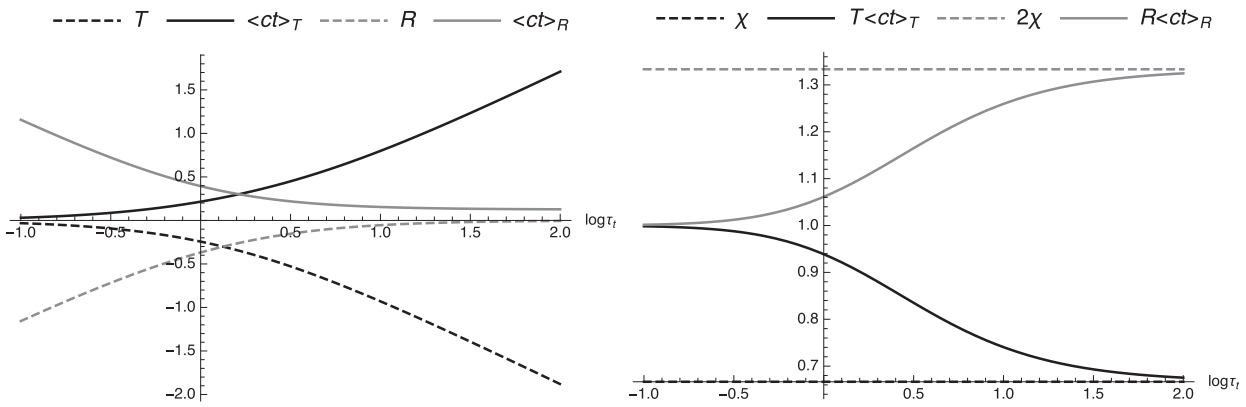

Fig. B.1. *Left:* $\log_{10}$ of 4 quantities in (25) versus $\log_{10}\tau_t$. *Right:* "*T*" & "*R*" terms.

Primarily with the inference of H in mind, the authors used the simplest possible model for the ratio $\langle ct\rangle_R/H$ based on isotropic illumination in the diffusion limit that comes hand-in-hand with the simple expression for R in (B.1). They show that

$$\langle ct\rangle_R/H = (2\chi)[1 + C_R(\tau_t/2\chi)], \tag{B.2}$$

where $C_R(x) = (x + 3/2)/2x(x + 1)$.

B.2. Transmission

For other purposes, such as predicting the waveform from cloud-to-ground lightning flashes as observed from space through an optically thick cloud, Davis and Marshak [44] did the same as in [43], but for transmitted light, thus obtaining a simple expression for the ratio $\langle ct\rangle_T/H$ based on isotropic illumination:

$$\langle ct\rangle_T/H = (\tau_t/2)[1 + C_T(\tau_t/2\chi)], \tag{B.3}$$

where $C_T(x) = (4x + 3)/2x(x + 1)$.

B.3. Reflection & transmission

Detailed derivations of all of the above expressions follow the same steps as laid out in Appendix A, and can be found in the review paper by Davis et al. [24] on diffusion of solar and laser radiation in plane-parallel media, as an idealized model for optically thick stratiform clouds. Apart from neglecting the $\partial F/\partial ct$ term in (A.4) to be in the framework of bone fide diffusion theory, the only differences are:

- no source terms in the continuity (A.3) or constituent (A.4) equations;
- instead the boundary/initial conditions in (A.5) and (A.6) become respectively $J(ct, 0) + 3\chi F(ct, 0) = 4\delta(ct)$ and $J(ct, H) - 3\chi F(ct, H) = 0$.

Therein is introduced the numerical extrapolation length factor χ as a control on the mixing of $J(ct, z)$ and $F(ct, z) = -(\ell_t/3)\partial J/\partial z$ in the Robin/3rd-type BCs of the simple Helmoltz ODE to solve (after Laplace transformations): $\left[(\mathrm{d}/\mathrm{d}z)^2 - a^2\right]\hat{J} = 0$ with $a^2 = 3k/\ell_t = 3(1-g)\sigma k$, and BCs $[1 \pm \chi\,\ell_t \mathrm{d}/\mathrm{d}z]\hat{J}|_{z=0(-),H(+)} = 4(-), 0(+)$.

Collecting all the above expressions pulled from Davis et al. [43,44], or [24], and recalling that $T(\tau_t) = 1 - R(\tau_t)$ in the absence of absorption, we can compute $\langle ct\rangle_F^{(\mathrm{all})}$ in (25). Light diffusion theory predicts that (25) adds up to $3\chi H$. This yields the expected result, $\langle ct\rangle_F^{(\mathrm{all})} = 2H$, if $\chi = 2/3$, which is the standard "Eddington" choice.

The left panel of Fig. B.1 displays the logs of all four of the quantities in (25) as functions of $\log_{10}\tau_t$, with $\tau_t = 1/10$ to 100, when $\chi = 2/3$ and $H = 1$. Note that diffusion theory does not apply in principle to media with $\tau_t \lesssim$ unity, but the validity of the expressions can be extended into that optically thin regime by varying the Eddington factor χ, in the limit of vanishingly small τ_t it increases from 2/3 to 4/3 (but not in this Figure). The right panel shows the transmitted and reflected contributions to $\langle ct\rangle_F^{(\mathrm{all})}$ in (25), with their asymptotic values.

References

[1] Intergovernmental Panel on Climate Change. Climate change 2013: The physical science basis. Cambridge (UK): Cambridge University Press; 2014.
[2] National Academies of SciencesEngineering, and Medicine. Thriving on our changing planet, a decadal strategy for earth observation from space. Washington (DC): The National Academies Press; 2018.
[3] NOAA National Environmental Satellite, Data, and Information Service (NESDIS). DSCOVR: Deep Space Climate Observatory; https://www.nesdis.noaa.gov/content/dscovr-deep-space-climate-observatory.
[4] Burt J, Smith B. Deep space climate observatory: the DSCOVR mission. In: Proceedings of the IEEE Aerospace Conference. IEEE; 2012. p. 1–13. doi:10.1109/AERO.2012.6187025.
[5] Marshak A, Herman J, Szabo A, Blank K, Cede A, Carn S, et al. Earth observations from DSCOVR/EPIC instrument. Bull Am Meteorol Soc 2018 (in press). doi:10.1175/BAMS-D-17-0223.1.
[6] NASA. DSCOVR: EPIC, Earth Polychromatic Imaging Camera; https://epic.gsfc.nasa.gov/.
[7] Davis AB, Merlin G, Cornet C, C-Labonnote L, Riédi J, Ferlay N, et al. Cloud information content in EPIC/DSCOVR's oxygen A- and B-band channels: an optimal estimation approach. J Quant Spectrosc Radiat Transf 2018;216:6–16. doi:10.1016/j.jqsrt.2018.05.007.
[8] Yang Y, Marshak A, Mao J, Lyapustin A, Herman J. A method of retrieving cloud top height and cloud geometrical thickness with oxygen A and B bands for the deep space climate observatory (DSCOVR) mission: radiative transfer simulations. J Quant Spectrosc Radiat Transf 2013;122:141–9. doi:10.1016/j.jqsrt.2012.09.017.
[9] Merlin G, Riédi J, C-Labonnote L, Cornet C, Davis AB, Dubuisson P, et al. Cloud information content analysis of multi-angular measurements in the oxygen A-band: application to 3MI and MSPI. Atmos Meas Tech 2016;9:4977–95. doi:10.5194/amt-9-4977-2016.
[10] Rodgers CD. Inverse methods for atmospheric sounding: Theory and practice. Singapore: World Scientific; 2000.
[11] Domoto GA. Frequency integration for radiative transfer problems involving homogeneous non-gray gases: the inverse transmission function. J Quant Spectrosc Radiat Transf 1974;14:935–42. doi:10.1016/0022-4073(74)90020-X.
[12] Lacis AA, Oinas V. A description of the correlated-*k* distribution method for modeling nongray gaseous absorption, thermal emission, and multiple scattering in vertically inhomogeneous atmospheres. J Geophys Res. Atmos 1991;96:9027–63. doi:10.1029/90JD01945.
[13] Goody RM, Yung YL. Atmospheric radiation: Theoretical basis. 2nd edition. Oxford (UK): Oxford University Press; 1995.
[14] Kratz DP. The correlated *k*-distribution technique as applied to the AVHRR channels. J Quant Spectrosc Radiat Transf 1995;53:501–17. doi:10.1016/0022-4073(95)90050-0.
[15] West R, Goody R, Chen L, Crisp D. The correlated-*k* method and related methods for broadband radiation calculations. J Quant Spectrosc Radiat Transf 2010;111:1672–3. doi:10.1016/j.jqsrt.2010.01.013.
[16] Young SJ. Band model theory of radiation transport. Reston (VA): The Aerospace Press; 2013.
[17] Modest MF. Radiative heat transfer. 3rd edition. Cambridge (MA): Academic Press; 2013.

[18] Conley AJ, Collins WD. Extension of the weak-line approximation and application to correlated-*k* methods. J Quant Spectrosc Radiat Transf 2011;112:1525–32. doi:10.1016/j.jqsrt.2011.02.008.
[19] Davis AB, Xu F, Diner DJ. Generalized radiative transfer theory for scattering by particles in an absorbing gas: addressing both spatial and spectral integration in multi-angle remote sensing of optically thin aerosol layers. J Quant Spectrosc Radiat Transf 2018;205:148–62. doi:10.1016/j.jqsrt.2017.10.003.
[20] Davis AB, Xu F, Diner DJ. Addendum to [JQSRT 205 (2018) 148162]. J Quant Spectrosc Radiat Transf 2018;206:251–3. doi:10.1016/j.jqsrt.2017.11.018.
[21] Davis AB. Multiple-scattering lidar from both sides of the clouds: addressing internal structure. J Geophys Res 2008;113:D14S10. doi:10.1029/2007JD009666.
[22] Irvine WM. The formation of absorption bands and the distribution of photon optical paths in a scattering atmosphere. Bull Astron Inst Neth 1964;17:226–79.
[23] van de Hulst HC. Multiple light scattering – Tables, formulas and applications, Vol. 2. San Diego (Ca): Academic Press; 1980.
[24] Davis AB, Polonsky IN, Marshak A. Space-time green functions for diffusive radiation transport, in application to active and passive cloud probing. In: Kokhanovsky AA, editor. Light Scattering Reviews, 4. Heidelberg (Germany): Springer-Praxis; 2009. p. 169–292. doi:10.1007/978-3-540-74276-0_5.
[25] Ferlay N, Thieuleux F, Cornet C, Davis AB, Dubuisson P, Ducos F, et al. Toward new inferences about cloud structures from multidirectional measurements in the oxygen A-band: middle-of-cloud pressure and cloud geometrical thickness from POLDER-3/PARASOL. J Appl Meteorol Climatol 2010;49:2492–507. doi:10.1175/2010JAMC2550.1.
[26] Bakan S, Quenzel H. Path length distributions of photons scattered in turbid atmospheres. Beiträge zur Physik der Atmosphäre 1976;49:272–84.
[27] Desmons M, Ferlay N, Parol F, Mcharek L, Vanbauce C. Improved information about the vertical location and extent of monolayer clouds from POLDER3 measurements in the oxygen A-band. Atmos Meas Tech 2013;6:2221–38. doi:10.5194/amt-6-2221-2013.
[28] Xu X, Wang J, Wang Y, J Zeng OT, Yang Y, Marshak A, et al. Passive remote sensing of altitude and optical depth of dust plumes using the oxygen A and B bands: first results from EPIC/DSCOVR at Lagrange-1 point. Geophys Res Lett 2017;44:7544–54. doi:10.1002/2017GL073939.
[29] Arridge SR. Optical tomography in medical imaging. Inverse Probl 1999;15:R41. doi:10.1088/0266-5611/15/2/022.
[30] Boas DA, Brooks DH, Miller EL, DiMarzio CA, Kilmer M, Gaudette RJ, et al. Imaging the body with diffuse optical tomography. IEEE Signal Process Mag 2001;18:57–75. doi:10.1109/79.962278.
[31] Blanco S, Fournier R. An invariance property of diffusive random walks. EPL (Europhys Lett) 2003;61:168. doi:10.1209/epl/i2003-00208-x.
[32] Pierrat R, Ambichl P, Gigan S, Haber A, Carminati R, Rotter S. Invariance property of wave scattering through disordered media. Proc Natl Acad Sci 2014;111:17765–70. doi:10.1073/pnas.1417725111.
[33] Savo R, Pierrat R, Najar U, Carminati R, Rotter S, Gigan S. Observation of mean path length invariance in light-scattering media. Science 2017;358:765–8. doi:10.1126/science.aan4054.
[34] Weiss GH. Some applications of persistent random walks and the telegrapher's equation. Phys A 2002;311:381–410. doi:10.1016/S0378-4371(02)00805-1.
[35] Polonsky IN, Davis AB. Off-beam cloud lidar: a new diffusion model and an analysis of LITE returns. Tech. Rep. LA-UR-05-0794. Los Alamos, NM: Los Alamos National Laboratory; 2005.
[36] Joseph JH, Wiscombe WJ, Weinman JA. The delta-eddington approximation for radiative flux transfer. J Atmos Sci 1976;33:2452–9. doi:10.1175/1520-0469(1976)033⟨2452:TDEAFR⟩2.0.CO;2.
[37] Roache PJ. Verification and validation in computational science and engineering. Albuquerque (NM): Hermosa Publishers; 1998.
[38] Mishchenko MI, Goldstein DH, Chowdhary J, Lompado A. Radiative transfer theory verified by controlled laboratory experiments. Opt Lett 2013;38:3522–5. doi:10.1364/OL.38.003522.
[39] Feller W. An introduction to probability theory and its applications, Vol. 2. New York (NY): Wiley; 1971.
[40] Redner S. A guide to first-passage processes. Cambridge (UK): Cambridge University Press; 2001.
[41] Akkermans E, Montambaux G. Mesoscopic physics of electrons and photons. Cambridge (UK): Cambridge University Press; 2007.
[42] Davis AB, Knyazihkin Y. A primer in 3D radiative transfer. In: Marshak A, Davis AB, editors. 3D Radiative Transfer in Cloudy Atmospheres. Heidelberg, Germany: Springer; 2005. p. 153–242.
[43] Davis AB, Cahalan RF, Spinhirne JD, McGill MJ, Love SP. Off-beam lidar: an emerging technique in cloud remote sensing based on radiative Green-function theory in the diffusion domain. Phys Chem Earth 1999;B24. doi:10.1016/S1464-1909(98)00034-3. 177–185 (Erratum 757–765).
[44] Davis AB, Marshak A. Space-time characteristics of light transmitted through dense clouds: a Green's function analysis. J Atmos Sci 2002;59:2713–27. doi:10.1175/1520-0469(2002)059⟨2713:STCOLT⟩2.0.CO;2.